NUMERICAL STUDY OF TURBULENT CHANNEL FLOW LADEN WITH FINITE-SIZE NON-SPHERICAL PARTICLES

Luca Brandt and Mehdi Niazi Ardekani
Linné FLOW Centre and SeRC
KTH Mechanics
SE 10044, Stockholm, Sweden
luca@mech.kth.se

Francesco Picano
Department of Industrial Engineering,
University of Padova,
Via Venezia 1, 35131 Padua, Italy

Pedro Costa and Wim-Paul Breugem
Laboratory for Aero & Hydrodynamics, TU-Delft,
Delft, The Netherlands

ABSTRACT

We present interface-resolved numerical simulations of turbulent channel flow laden with non-spherical rigid and neutrally-buoyant particles. We first focus on the case of oblate particles of aspect ratio 1/3 at volume fractions up to 15% and show that the turbulent drag is decreasing when increasing the particle volume fraction although the effective viscosity of the suspension actually increases. We relate the observed drag reduction to turbulence attenuation and to particle migration away from the near-wall region. Particles tend to align parallel to the wall with rotation rates significantly lower than those reported for spheres. In the second part of the study, we examine the effect of the particle slenderness on the observed drag reduction and show that the drag increases for flatter particles.

INTRODUCTION

The presence of the finite-size particles (particles larger than the smallest hydrodynamic scales of the flow) can alter the turbulent structures at or below the particle size. A few studies in recent years have investigated dense suspensions in highly inertial regime for spherical particles. Matas *et al.* (2003); Yu *et al.* (2013); Lashgari *et al.* (2015) reported a decrease of the critical Reynolds number for transition to turbulence in the semi-dilute regime. Shao *et al.* (2012) performed numerical simulations, revealing a decrease of the fluid streamwise velocity fluctuations due to an attenuation of the large-scale streamwise vortices in a turbulent channel flow. Recently, Picano *et al.* (2015) studied dense suspensions of neutrally-buoyant particles in turbulent channel flow up to volume fraction $\phi = 20\%$. These authors reported that the velocity fluctuation and the Reynolds shear stress gently increase with ϕ before sharply decreasing at $\phi = 20\%$, even though the overall drag still increases. They attribute the overall drag increase to the effect of particle-induced stresses which compensate the Reynolds stress reduction at high ϕ. At lower ϕ, in the fully turbulent regime, Costa *et al.* (2016) have shown that the formation of a particle wall layer is responsible for the observed drag increase; assuming two distinct transport mechanisms in this near-wall layer and in the bulk, these authors define an effective wall location such that the flow in the bulk can still be accurately described by an effective suspension viscosity. This allows to derive scaling laws for the mean velocity profile of the suspension flow, together with a master equation able to predict the increase in drag as function of the particle size and volume fraction (see Costa *et al.*, 2016, for more details).

Despite these previous efforts, the turbulent flow of finite-size non-spherical particles is still unexplored. In this work we perform simulations of turbulent channel flow in the presence of oblate particles, investigating the effect of the particle shape on the turbulence modulation.

NUMERICAL METHOD AND SETUP

The simulations are performed with an extended version of the direct-forcing immersed boundary method initially developed by Breugem (2012). With this approach, a Lagrangian mesh is used to track the solid object whereas the flow is solved on a fixed Eulerian mesh. In particular, we use a classic second-order finite-volume approach with pressure correction. The method has been validated against several tests cases for the simulations of spherical particles (see Lambert *et al.*, 2013; Picano *et al.*, 2013; Lashgari *et al.*, 2016) and extended for spheroidal particles by Ardekani *et al.* (2016).

When the distance between the particles or one particle and the wall is below one grid cell a lubrication correction, based on asymptotic analytical solutions, is used to resolve the short-range forces. Collisions between particles are treated with a soft-sphere collision model, including friction and tangential collisions, see the full description in Costa *et al.* (2015). For the case of non-spherical particles, short-range interactions are computed assuming spherical particles with radius equal to the radius of curvature at contact of each spheroidal particle and same total

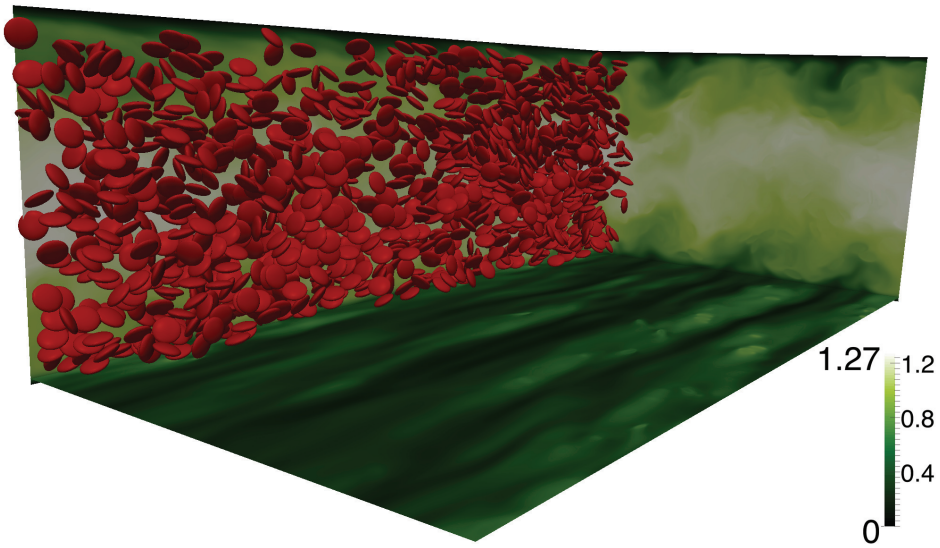

Figure 1. Instantaneous visualization of the turbulent channel flow of a suspension of oblate particles at volume fraction $\phi = 0.15$. The color contours represent the streamwise velocity on three orthogonal planes. Only particles over 1/9 of the domain are shown for clarity.

mass. Details about the implementation, together with validation against Jeffery orbits and settling spheroids, can be found in Ardekani *et al.* (2016).

We study a pressure-driven channel flow in a computational domain of size $L_x = 6h$, $L_y = 2h$ and $L_z = 3h$ in the streamwise, spanwise and wall-normal directions. The bulk velocity U_b is fixed to attain a bulk Reynolds number $Re_b = 2hU_b/\nu = 5600$ corresponding to a friction Reynolds number $Re_\tau = U_* h/\nu = 180$ for the single phase flow, with ν, the kinematic viscosity of the fluid phase and $U_* = \sqrt{\tau_w/\rho_f}$, the friction velocity, calculated with the shear stress τ_w at the wall. Periodic boundary conditions are imposed in the streamwise and spanwise directions while a no slip and no penetration boundary condition at the walls.

We consider non-Brownian neutrally-buoyant rigid spheroidal particles with aspect ratio $\mathscr{AR} = 1/2, 1/3, 1/4$ and $1/5$ (ratio of polar over equatorial radius). The particle equivalent diameter D_{eq}, i.e. the diameter of a sphere with same volume, is set to $h/D_{eq} = 9$ to compare with the results of Picano *et al.* (2015) for spheres. The size of the computational domain is therefore $54 \times 18 \times 27$ in units of D_{eq}. The maximum and minimum diameters of the oblate particle with $\mathscr{AR} = 1/3$ are $D_1 = h/6.24$ and $D_2 = h/18.72$. At this aspect ratio, we perform simulations at four different volume fractions $\phi = 5$; 7.9; 10; 15%. The volume fractions 5%, 10% and 15% correspond to 2500, 5000 and 7500 particles in our computational domain. To study the effect of particle aspect ratio, we consider the same bulk Reynolds number, box size and particle equivalent diameter while fixing the volume fraction to $\phi = 10\%$. The maximum and minimum diameters of the oblate particle with $\mathscr{AR} = 1/5$ are $D_1 = h/5.26$ and $D_2 = h/26.33$.

The resolution adopted is 32 grid points for D_{eq} for spheres and oblates of aspect ratios 1/2 and 1/3. For the particles of aspect ratios 1/4 and 1/5 we have used 48 for D_{eq}, corresponding to a resolution of $2592 \times 864 \times 1296$ in our computational domain. The numbers of Lagrangian points needed on a single particle are 3219, 3406, 3720, 9120, 9878 for the aspect ratios 1, 1/2, 1/3, 1/4, 1/5.

RESULTS

Oblate particles of aspect ratio 1/3

Figure 1 displays the turbulent channel flow with oblate particles ($\mathscr{AR} = 1/3$) from the simulations at largest volume fraction. For clarity, particles are shown only over one portion of the computational domain. The most interesting result is reported in figure 2 where we display the percentage of drag reduction versus the volume fraction. This is measured taking as reference the drag of the single-phase flow ($Re_\tau = 180$). Although the effective viscosity of the suspension increases with the particle volume fraction, the total suspension drag clearly decreases as soon as $\phi > 5\%$: the drag reduces by 8% when $\phi = 15\%$, the largest volume fraction considered. The observed drag reduction is in contrast to what observed in the case of spherical particles, where the presence of the particle wall layer and the increasing importance of particle induced stresses leads to drag increase for the large datasets considered, see Costa *et al.* (2016).

The observed drag reduction can be related to a reduction of the turbulence activity, as documented in figure 3 where we report the wall-normal profiles of the turbulent kinetic energy for the different cases under consideration. Here, one can see that the fluctuations decrease close to the wall for increasing particle volume fraction. When comparing with the single phase flow, we also observe a slight increase in the channel centre, however non monotonic with the particle volume fraction. Analysis of the different components of the turbulent kinetic energy also reveal a more isotropic turbulence (see also Ardekani *et al.*, 2017).

Particle migration is known to play a role in laminar flows of suspensions and we therefore show in Figure 4 the local particle volume fraction versus the wall-normal distance for the different cases under investigation. The data reveal particle migration away from the wall as the value of the volume fraction increases in the core of the channel above the nominal value, used in the figure to normalize the profiles. Interestingly, the same effect is not observed in laminar flows, as reported in Ardekani *et al.* (2017). More

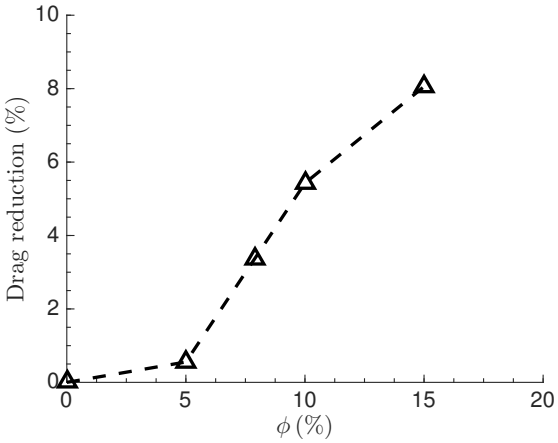

Figure 2. Percentage of drag reduction versus the volume fraction of oblate particles with $\mathscr{AR} = 1/3$. The reference zero value pertains the single-phase flow at same conditions ($Re_\tau = 180$).

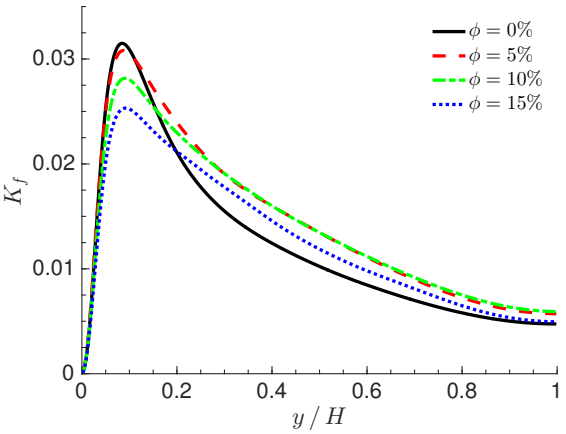

Figure 3. Wall-normal (y) profiles of the turbulent kinetic energy of the fluid phase for the different volume fractions under investigation. Oblate particles of aspect ratio $\mathscr{AR} = 1/3$ and bulk Reynodls number $Re_b = 5600$.

relevant to the case of a turbulent flow, we see that the particle wall-layer observed in suspensions of spherical particles, a layer of increased concentration close to the wall with thickness of the order of the particle diameter, is absent in the case of oblate particles. As mentioned above, this particle wall-layer is responsible for the increase of the drag of the suspension flow, see Costa *et al.* (2016).

Finally, we analyze the budget of streamwise momentum transport. This is obtained by phase and ensemble averaging the streamwise momentum equations. For the full derivation the reader is referred to Zhang & Prosperetti (2010) for the original derivation and to Picano *et al.* (2015) for an extension to the case of turbulent channel flow, exploiting the streamwise and spanwise flow homogeneity. In

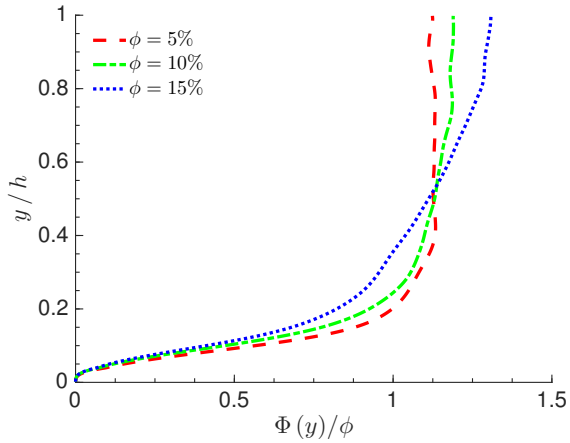

Figure 4. Wall-normal (y) profiles of the particle local volume fraction, normalized with the nominal value reported in the legend.

this case, the momentum budget reduces to

$$\tau/\rho_f = U_*^2\left(1-\frac{y}{h}\right) = \nu(1-\Phi)\frac{\mathrm{d}U_f}{\mathrm{d}y} - \left[\Phi\langle u_p' v_p'\rangle + (1-\Phi)\langle u_f' v_f'\rangle\right] + \frac{\Phi}{\rho}\langle\sigma_{xy}^p\rangle \tag{1}$$

The expression above shows that the momentum is trasferred by three different mechanisms: viscous stresses, Reynolds stresses (pertaining the fluid and particle motions) and particle-induced stresses, including collisions and lubrication forces. An overview of the relevance of the different contributions to the overall momentum transfer versus the particle volume fraction and the bulk Reynolds number is reported in Lashgari *et al.* (2014, 2016) for spherical particles larger than those considered here. These authors show that the flow is dominated by viscous stresses for low Reynolds number and relatively low volume fractions, by the Reynolds stresses at the highest Reynolds numbers considered in that study ($Re_b = 5000$) and $\phi < 10\%$, and by the particle-induced stresses at higher volume fractions.

While this previous study covered laminar and turbulent flows, we focus here on the turbulent regime. The wall-normal integral of the different contributions provides the relative importance of each term. This is depicted in figure 5 for the four cases under investigation, normalized with the pressure forcing of the single-phase flow. The diagram shows that while the viscous contribution is almost independent of the volume fraction ϕ, the contribution from the Reynolds stresses significantly decreases when increasing the number of particles. This decrease is only partially compensated by the particle-induced stresses, unlike the case of spherical particles where the drag is found to increase despite the reduction of turbulent stress because of the particle-induced stress (Lashgari *et al.*, 2014; Picano *et al.*, 2015).

Using a quadrant analysis, we calculate the contribution of each quadrant to the Reynolds shear stress denoted as Q_1 ($u' > 0, v' > 0$), Q_2 ($u' < 0, v' > 0$), Q_3 ($u' < 0, v' < 0$) and Q_4 ($u' > 0, v' < 0$). Q_2 and Q_4 events are associated with positive Reynolds shear stress and thus positive turbulent kinetic energy production. These observable corre-

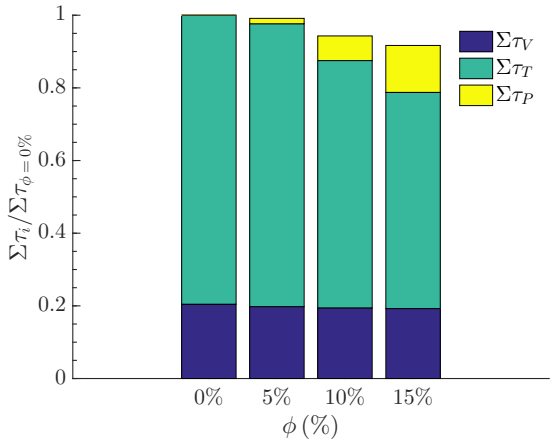

Figure 5. Momentum budget. Relative contribution of the turbulent stresses $\Sigma\tau_T$ (green), viscous stresses $\Sigma\tau_V$ (blue) and particle-induced stresses $\Sigma\tau_P$ (yellow) for the different volume fractions under investigation.

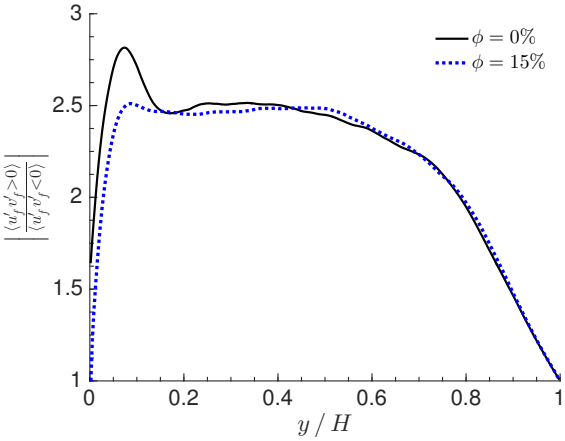

Figure 6. Positive over negative production of the Reynolds shear stress for the fluid phase versus y/h.

spond to the ejection and sweep events of near-wall turbulence, respectively. The Q_1 and Q_3 events, on the other hand, are responsible for negative Reynolds shear stress and quenching of turbulence. We display in figure 6 the ratio between the total positive and negative contribution to the Reynolds stresses for the oblate case at volume fraction $\phi = 15\%$, and compare them with the single phase flow. It can be concluded from this figure that oblate particles effectively damp the ejection and sweep events close to the wall as the peak is almost absent for the particulate case.

The observed turbulence attenuation is therefore specific to the dynamics of the non-spherical particles. Figure 7 displays the particle mean orientation versus the wall-normal distance. The data clearly show that, close to the wall, the particles are on average parallel to the wall, thus creating a separation between the near-wall cycle and the bulk of the flow. In addition, the results in Ardekani *et al.* (2017) indicate that the average spanwise rotation rate is significantly lower for oblate particles than for spherical particles.

The reasons behind the absence of the particle layer and of the reduced rotation rate are investigated examining

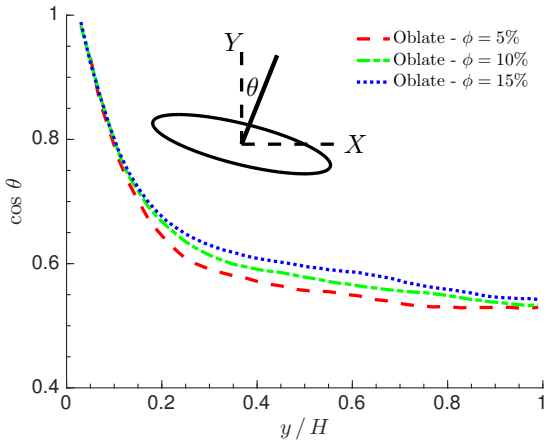

Figure 7. Cosine of the mean particle inclination angle, θ, measured with respect to the wall, versus y/h.

the average force and torque for the case with volume fraction $\phi = 15\%$. We compute the mean drag force F_D, lift force F_L and spanwise torque T_z acting on the particles as a function of distance to the wall, y/h, and of the streamwise component of the particle orientation vector $\hat{o}_p^x$. The orientation vector $\hat{o}_p$ is defined as unit vector parallel to the particle symmetric axis and pointing towards the channel center. Contours of the normalized lift F_L are depicted in figure 8(a). The results (considering also torque and drag) show that when the particles are sufficiently close to the wall (i.e. in the region of high mean velocity gradients), the forces and the torques acting on the particle change according to their orientation as sketched in 8(b). Particles, on average, have a negative spanwise angular velocity due to the mean flow gradient and the analysis presented here, interestingly, indicates that when these have a positive orientation, $\hat{o}_p^x > 0$, they are lifted by the flow towards the channel center whereas the opposite is true when they have a negative $\hat{o}_p^x$. It is important to note that the magnitude of the upward lift is significantly larger than the downward force. This difference in magnitude can explain the absence of the particle wall layer in the case of oblate particles. It can be concluded from figure 8(b) that particles near the wall with an inclination with negative $\hat{o}_p^x$ tend to be aligned by the flow parallel to the wall and accelerate towards it; particles with positive $\hat{o}_p^x$, conversely, are accelerated towards the channel center by hydrodynamic interactions. This indicates that oblate particles are most likely parallel to the wall in its vicinity. This is therefore a stable configuration, which has apparently important implications for drag reduction.

Oblate particles of different aspect ratio

Finally, we examine the effect of changing the particle aspect ratio. Figure 9 displays the percentage of drag reduction versus the particle aspect ratio for the volume fraction $\phi = 10\%$. The reference zero value pertains the single-phase flow at same conditions. The drag of spherical particles ($\mathscr{AR} = 1$) is about 18% larger than for the single phase flow whereas the most slender oblate particles ($\mathscr{AR} = 5$) result in a reduction of about 12%. The drag of suspensions of particles with aspect ratio 2 almost matches the case of the single phase fluid. In this case, the reduction of turbulence production due to the particle dynamics al-

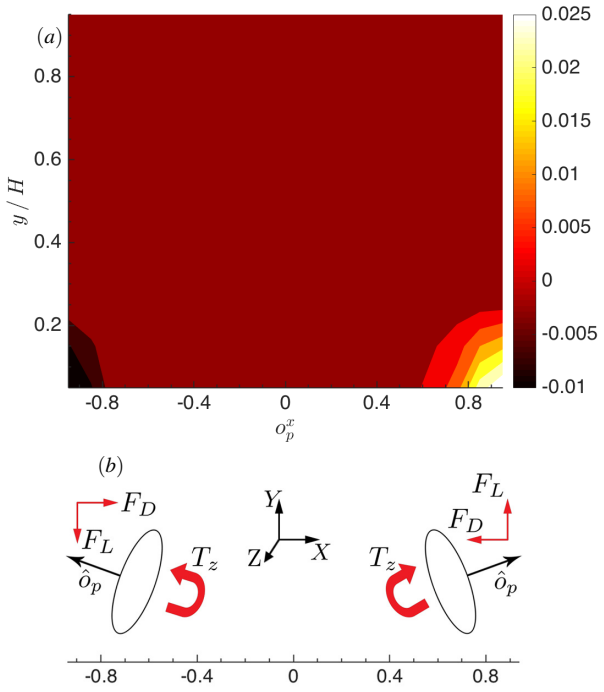

Figure 8. (a) Contours of the lift force acting on the particles at $\phi = 15\%$ as a function of distance to the wall, y/h, and the streamwise component of the particle orientation vector $\hat{o}_p^x$. (b) A schematic of the action of the forces and torques for the cases of positive and negative $\hat{o}_p^x$.

most balances the increase of the suspension viscosity. The momentum budget pertaining cases with different particle aspect ratios is reported in figure 10. The data in the figure indicate that viscous stresses and particle stresses are almost independent of the aspect ratio at constant volume fraction. The turbulent Reynolds stresses however decrease when increasing the particle slenderness, consistent with the explanation for the drag reduction discussed above.

SUMMARY AND OUTLOOK

We present interface-resolved numerical simulations of turbulent channel flow laden with non-spherical rigid and neutrally-buoyant particles. First, we report results for oblate particles of aspect ratio 1/3 at volume fractions up to 15%. We show here that the drag of the flow is decreasing when increasing the particle volume fraction although the effective viscosity of the suspension actually increases. The drag reduces by 8% when $\phi = 0.15$ although the effective viscosity of the suspension increases by 56%. With respect to the single-phase flow, the drag is reduced and the turbulent fluctuations attenuated in the presence of oblate spheroids. In particular, the turbulence activity decreases to lower values than those obtained by accounting only for the effective suspension viscosity. To explain the observed drag reduction, we consider the particle dynamics and the interactions of the particles with the turbulent velocity field and show that the particlewall layer, previously observed and found to be responsible for the increased dissipation in suspensions of spheres, disappears in the case of oblate particles. These rotate significantly slower than spheres near the wall (Ardekani *et al.*, 2017) and tend to stay with their

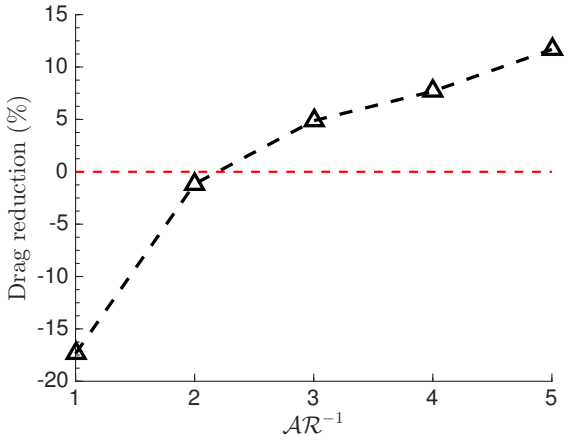

Figure 9. Percentage of drag reduction versus the particle aspect ratio for volume fraction $\phi = 10\%$. The reference zero value pertains the single-phase flow at same conditions ($Re_\tau = 180$).

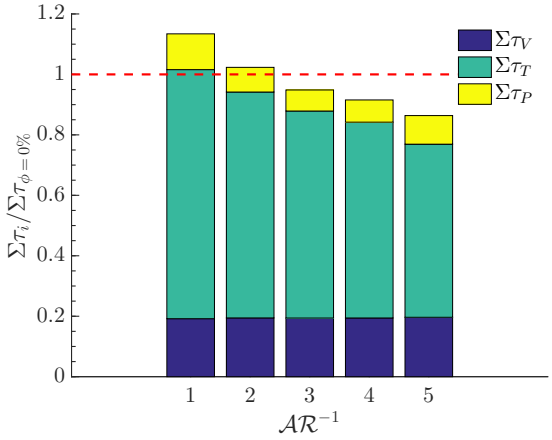

Figure 10. Momentum budget. Relative contribution of the turbulent stresses $\Sigma\tau_T$ (green), viscous stresses $\Sigma\tau_V$ (blue) and particle-induced stresses $\Sigma\tau_P$ (yellow) for the different particle aspect ratios under investigation.

major axes parallel to the wall, which leads to a decrease of the Reynolds stresses and turbulence production and so to the overall drag reduction. The turbulence attenuation is also related to particle migration away from the near-wall region.

It is interesting to add here that simulations have been also performed allowing the particles to translate while keeping them parallel to the wall. In this case, the drag reduces even more (18% at $\phi = 10\%$) and so the turbulent fluctuations. Indeed, the oblate disc-like particles tend to form a shield between the near-wall region and bulk of the flow. Simulations performed for different particle aspect ratios show that the turbulence attenuation increases with the particle slenderness, confirming the mechanisms discussed above.

The present study is part of an ongoing effort aiming to understand the turbulent flow of particle suspensions, with particles larger than the smallest turbulent eddies. Several effects need to be considered to gain better understanding of the complex physics governing this multiscale prob-

lem. Among them, particle size and distribution, deformability, density and shape. The effect of the particle size is discussed in Costa *et al.* (2016), although simulations of smaller and smaller particles are computationally very expensive. Simulations of particles with different densities, while neglecting gravity, are presented in Fornari *et al.* (2016) to disentangle the effect of particle and fluid inertia. The results of this study indicate that the flow is governed by the particle volume fraction, excluded volume effects, for density ratios lower than 10. A similar conclusion is reported by Lashgari *et al.* (2017) who studied binary mixtures of particles of different sizes. Despite some weak segregation of smaller particles close to the wall, the flow statistics are mainly determined by the total particle volume fraction.

The results presented here show that particle shape can have a significant impact on the suspension behaviour. Prolate particles will therefore need to be studied, in addition to fibers and filaments, either rigid or flexible. Anisotropic particles also promise to reveal new interesting physics as recently shown for the case of sediments (Goldfriend *et al.*, 2017). Future efforts will have to consider particle deformability as well, as this can result in significant modifications of the particle shape.

REFERENCES

Ardekani, M. N., Costa, P., Breugem, W. P. & Brandt, L. 2016 Numerical study of the sedimentation of spheroidal particles. *International Journal of Multiphase Flow* **87**, 16–34.

Ardekani, M. N., Costa, P., Breugem, W. P., Picano, F. & Brandt, L. 2017 Drag reduction in turbulent channel flow laden with finite-size oblate spheroids. *Journal of Fluid Mechanics* **816**, 43–70.

Breugem, W-P. 2012 A second-order accurate immersed boundary method for fully resolved simulations of particle-laden flows. *Journal of Computational Physics* **231** (13), 4469–4498.

Costa, P., Boersma, B. J., Westerweel, J. & Breugem, W. P. 2015 Collision model for fully resolved simulations of flows laden with finite-size particles. *Physical Review E* **92** (5), 053012.

Costa, P., Picano, F., Brandt, L. & Breugem, W. P. 2016 Universal scaling laws for dense particle suspensions in turbulent wall-bounded flows. *Physical review letters* **117** (25), 134501.

Fornari, W., Formenti, A., Picano, F. & Brandt, L. 2016 The effect of particle density in turbulent channel flow laden with finite size particles in semi-dilute conditions. *Phys. Fluids* **28**, 033301.

Goldfriend, Tomer, Diamant, Haim & Witten, Thomas A. 2017 Screening, hyperuniformity, and instability in the sedimentation of irregular objects. *Phys. Rev. Lett.* **118**, 158005.

Lambert, Ruth A, Picano, Francesco, Breugem, Wim-Paul & Brandt, Luca 2013 Active suspensions in thin films: nutrient uptake and swimmer motion. *J. Fluid Mech.* **733**, 528–557.

Lashgari, I., Picano, F. & Brandt, L. 2015 Transition and self-sustained turbulence in dilute suspensions of finite-size particles. *Theoretical and Applied Mechanics Letters* **5** (3), 121–125.

Lashgari, I., Picano, F., Breugem, W. P. & Brandt, L. 2014 Laminar, turbulent, and inertial shear-thickening regimes in channel flow of neutrally buoyant particle suspensions. *Physical review letters* **113** (25), 254502.

Lashgari, I., Picano, F., Breugem, W. P. & Brandt, L. 2016 Channel flow of rigid sphere suspensions: particle dynamics in the inertial regime. *International Journal of Multiphase Flow* **78**, 12–24.

Lashgari, Iman, Picano, Francesco, Costa, Pedro, Breugem, Wim-Paul & Brandt, Luca 2017 Turbulent channel flow of a dense binary mixture of rigid particles. *Journal of Fluid Mechanics* **818**, 623–645.

Matas, J. P., Morris, J. F. & Guazzelli, E. 2003 Transition to turbulence in particulate pipe flow. *Physical review letters* **90** (1), 014501.

Picano, F., Breugem, W. P. & Brandt, L. 2015 Turbulent channel flow of dense suspensions of neutrally buoyant spheres. *Journal of Fluid Mechanics* **764**, 463–487.

Picano, F., Breugem, W. P., Mitra, D. & Brandt, L. 2013 Shear thickening in non-brownian suspensions: an excluded volume effect. *Physical review letters* **111** (9), 098302.

Shao, X., Wu, T. & Yu, Z. 2012 Fully resolved numerical simulation of particle-laden turbulent flow in a horizontal channel at a low reynolds number. *Journal of Fluid Mechanics* **693**, 319–344.

Yu, Z., Wu, T., Shao, X. & Lin, J. 2013 Numerical studies of the effects of large neutrally buoyant particles on the flow instability and transition to turbulence in pipe flow. *Physics of Fluids (1994-present)* **25** (4), 043305.

Zhang, Q. & Prosperetti, A. 2010 Physics-based analysis of the hydrodynamic stress in a fluid-particle system. *Physics of Fluids (1994-present)* **22** (3), 033306.